

GLOBAL BIFURCATION OF CAPILLARY-GRAVITY DARK SOLITARY WAVES ON THE SURFACE OF A CONDUCTING FLUID UNDER NORMAL ELECTRIC FIELDS

by A. Doak

(Department of Mathematical Sciences, University of Bath, Bath BA2 7AY)

T. Gao[‡]

*(School of Computing and Mathematical Sciences, University of Greenwich, London SE10
9LS)*

J.-M. Vanden-Broeck

(Department of Mathematics, University College London, London WC1E 6BT, UK)

[Received May 9, 2022]

Summary

This paper is concerned with capillary-gravity waves travelling on the interface of a dielectric gas and a conducting fluid under the effect of a vertical electric field. A boundary integral equation method is employed to compute fully nonlinear steady travelling wave solutions. The global bifurcation diagram of periodic waves, solitary waves, generalised solitary waves and dark solitary waves is presented and discussed in detail.

1. Introduction

Electrohydrodynamics (EHD) concerns the coupled motion of fluids and electric fields. It enjoys numerous chemical and engineering applications as electric fields can be used to manipulate fluid flows in desirable ways. For example, coating processes (**1**, **2**), electrospray technology (**3**) and cooling systems in high-performance electrical devices with the help of conducting fluids (**4**) are among those important industrial applications. The readers are referred to (**5**, **6**) for a review.

In practice, an EHD problem is usually concerned with an interface between two fluids in which gravity and surface tension are both considered. A good understanding of the fluid dynamics from a mathematical perspective is significantly helpful to engineers in enhancing and innovating the design of industrial products. Early works on EHD can be traced back to (**7**), where normal electric fields were shown theoretically and experimentally to be capable of destabilising an interface between a conducting fluid and a dielectric gas. Later (**8**) performed a linear stability analysis on the interfacial flow under the effects of electric fields imposed tangentially to the undisturbed interface, and discovered that waves with short wavelengths may be regularised. These two early works were followed by numerous

[‡] Email address for correspondence: t.gao@gre.ac.uk

extensions regarding fluid instabilities, e.g. (9, 10, 11). The former two papers utilised reduced model equations whereas the latter one used direct numerical simulations.

Studying travelling waves propagating on the interface is equally important in understanding the nature of the fluid dynamics. In the absence of the electric fields, the problem is reduced to the classic capillary-gravity flow. Fully nonlinear solutions to the Euler equations were computed by (12, 13, 14, 15) for solitary waves, (16) for generalised solitary waves, (17) for asymmetric solitary waves (18) for asymmetric generalised solitary waves, and a complete bifurcation diagram of the solitary waves was presented in (19). In the presence of normal electric fields, weakly nonlinear model equations were derived for analysis and simulation under the assumption of small wave amplitude, e.g. Boussinesq-type equations by (28), and a Benjamin equation by (20) later generalised to a two-dimensional model by (21). Furthermore, by truncating Dirichlet-to-Neumann operators, (23) derived a Hamiltonian model accurate up to fifth-order in the amplitude parameter. A detailed summary was written by (22) where various models were derived. Fully nonlinear computations were achieved by a boundary integral equation method or equivalent in (29, 30, 31, 32). In particular, the work by (32) studied the general setting in which both the gas and fluid are dielectrics.

The bifurcation of solitary waves at small amplitude can oftentimes be investigated by weakly nonlinear models. Such a bifurcation can occur at the global extremum of the linear dispersion relation, and when such a point occurs for finite wavenumber, the local bifurcation structure is predicted by the Nonlinear Schrödinger (NLS) Equation (33). In the absence of electric fields, the associated NLS is of the focussing type which predicts the existence of solitary wavepacket whose wave phase speed and group speed are identical. As shown by (22), for a certain range of strength of the electric field, the NLS changes to the defocussing type whose only solitary wave solutions are the so-called dark solitary waves (a decaying centre and non-decaying oscillatory far-field). The local bifurcation structure was found to higher orders of accuracy (i.e. higher nonlinearity) by (23). We note that a similar local bifurcation was found in the context of interfacial gravity-capillary waves with uniform background flows under the effect of horizontal electric fields in a recent work (34).

In this paper, we will explore the complete bifurcation structure of solitary waves to the fully nonlinear system, and contrast it with that of the reduced NLS model. It is achieved by numerically computing fully nonlinear travelling wave solutions via a boundary integral equation method, in which no smallness assumption on the amplitude is required, to extend the results from (23) where the local bifurcations were studied. The rest of the article is organised as follows. In section 2, the detailed formulation of the problem is demonstrated. The numerical scheme is explained in section 3. The numerical results are presented and discussed in section 4. Concluding remarks are made in section 5.

2. Formulation

An irrotational flow of an inviscid and incompressible fluid of density ρ is considered in a two-dimensional space under the effect of gravitational force, surface tension and a vertical electric field. The fluid is bounded above by a gas layer. We assume both regions to be of infinite depth. This assumption implies that the wave lengthscale is significantly shorter than the depth of both the fluid and gas layers. Due to the presence of capillarity, the wave lengthscale is of millimeters. Furthermore, the fluid is usually treated as a perfect conductor whereas the gas is a dielectric since the conductivity of the former is much larger

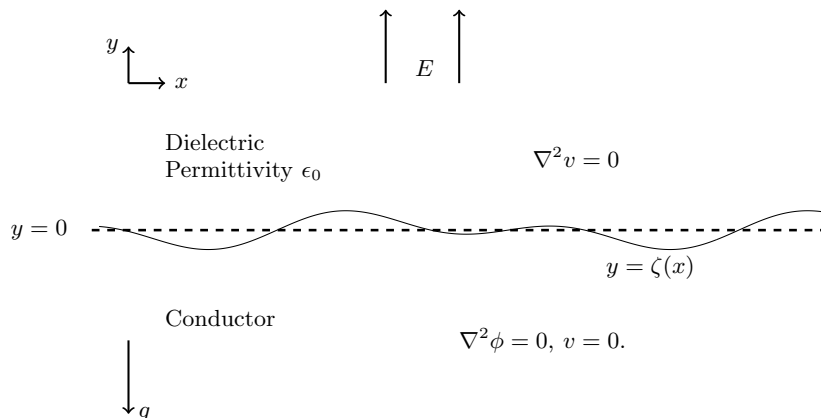


Fig. 1 Configuration of the problem. The gravity acts in the negative y -direction. We denote the equation of the unknown free surface by $y = \zeta(x)$.

than that of the latter. We adopt such a setting, and denote the permittivity of the gas by ϵ_0 . The gravitational constant and the surface tension coefficient are denoted by g and σ respectively. We introduce a Cartesian x - y coordinate system in which the gravity points in the negative y -direction. All the waves are assumed to propagate with constant speed in the positive x -direction. A reference frame moving with the wave is chosen such that the solution becomes steady, and hence no time derivative is concerned. A voltage potential v induced by the vertical electric field has asymptotic behaviour $v \sim V_0 y$ as $y \rightarrow \infty$. The interface between the fluid and the gas is denoted by $y = \zeta(x)$ whose mean level is fixed at $y = 0$. Due to the incompressible assumption, the velocity vector can be expressed in terms of the gradient of a scalar (velocity) potential ϕ . The system of equations then becomes

$$\nabla^2 \phi = 0, \quad \text{for } y < \zeta(x), \quad (2.1)$$

$$\nabla^2 v = 0, \quad \text{for } y > \zeta(x), \quad (2.2)$$

$$\phi_y = \phi_x \zeta_x, \quad \text{on } y = \zeta(x), \quad (2.3)$$

$$v = 0, \quad \text{on } y = \zeta(x), \quad (2.4)$$

$$v_y \rightarrow 1, \quad \text{as } y \rightarrow \infty, \quad (2.5)$$

$$\phi_y \rightarrow 0, \quad \text{as } y \rightarrow -\infty, \quad (2.6)$$

and

$$|\nabla \phi|^2 + y - \frac{\zeta_{xx}}{(1 + \zeta_x^2)^{3/2}} - \frac{E_b}{2(1 + \zeta_x^2)} [(1 - \zeta_x^2)(v_x^2 - v_y^2) + 4\zeta_x v_x v_y] = 0, \quad \text{on } y = \zeta(x), \quad (2.7)$$

where we have chosen

$$\left(\frac{\sigma}{\rho g}\right)^{\frac{1}{2}}, \quad \left(\frac{\sigma}{\rho g^3}\right)^{\frac{1}{4}}, \quad V_0, \quad (2.8)$$

as the reference length, time and voltage potential. The subscripts denote partial derivatives. A schematic of the flow configuration is depicted in Fig. 1. The non-dimensional electric parameter E_b is given by

$$E_b = \epsilon_0 V_0^2 \sqrt{\rho g / \sigma^3}. \quad (2.9)$$

It is a measure of the ratio of electric forces over the forces due to gravity or capillarity. Equation (2.6) is the zero flow condition at infinity. Equation (2.3) and (2.7) are the kinematic and the dynamic boundary condition respectively. Condition (2.4), obtained from the conducting nature of the fluid, implies

$$v_x = -v_y \zeta_x, \quad \text{on } y = \zeta(x), \quad (2.10)$$

which simplifies (2.7) as

$$|\nabla\phi|^2 + y - \frac{\zeta_{xx}}{(1 + \zeta_x^2)^{3/2}} - \frac{E_b}{2} |\nabla v|^2 = 0, \quad \text{on } y = \zeta(x). \quad (2.11)$$

Upon linearising the system and seeking perturbations of phase speed c_p and wavenumber k , one recovers a linear dispersion relation of the form

$$c_p^2 = \frac{\omega^2}{k^2} = \frac{1}{k} + k - E_b, \quad (2.12)$$

Linear stability is given by the sign of c_p : when it is positive (negative), the system is linearly stable (unstable). It can be seen that for $E_b < 2$, the flow is always linearly stable, and there exists a phase speed minimum at $k = k_c = 1$ regardless the value of E_b . However, when $E_b > 2$, a flow destabilisation takes place for k in a certain range in which c_p^2 turns to be negative. An illustrating graph is plotted in Fig. 2.

Due to the assumption that waves travel with constant speed, one can still recover periodic solutions with wavenumber k when the system is unstable, given $c_p(k)$ is real. Such solutions are of course linearly unstable. For solitary waves, there are two candidates for bifurcation along the dispersion relation: the long-wave speed ($k = 0$), and the minimum ($k = 1$). At $k = 0$, one expects to find generalised solitary waves, due to the resonance with a finite wavelength linear wave with the same speed (for example, see **(13, 16)** for such solutions with $E_b = 0$). On the other hand, at the minimum, one expects to find solitary wave packets, described at small amplitude by the NLS equation (see below). In this paper, we focus on solutions which bifurcate from the minimum. Hence, we restrict our attention to $E_b < 2$.

2.1 Weakly nonlinear theory

Solitary wavepacket solutions are known to bifurcate from the minimum of the dispersion relation, such as in the numerical solutions found in **(36)** for $E_b = 0$. It was shown in **(33)** that such a bifurcation is predicted by the Nonlinear Schrödinger (NLS) equation. The associated NLS for the system (2.1)-(2.7) was derived via normal form analysis by **(22, 23)** by writing ϕ and ζ as a series in powers of ϵ which is a small parameter as follows

$$\zeta = \epsilon A(X, \tau) e^{i(kx - \omega t)} + \text{c.c.} + \epsilon^2 \zeta_2 + \epsilon^3 \zeta_3 + \dots, \quad (2.13)$$

$$\phi = \epsilon B(X, \tau) e^{i(kx - \omega t)} + \text{c.c.} + \epsilon^2 \phi_2 + \epsilon^3 \phi_3 + \dots, \quad (2.14)$$

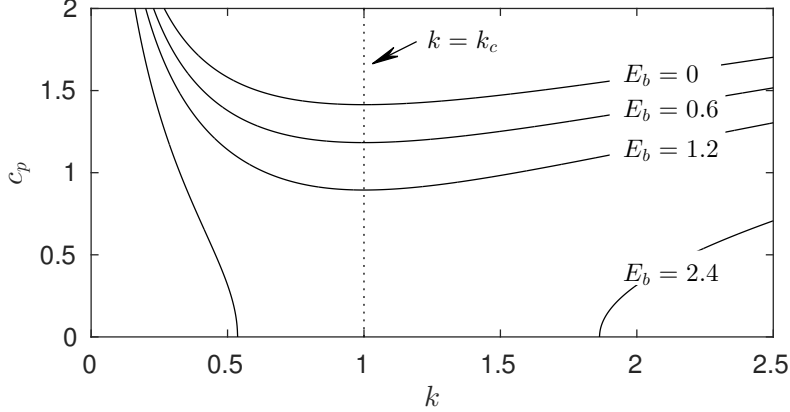


Fig. 2 Plot of c_p versus k as in (2.12) for $E_b = 0, 0.6, 1.2$ and 2.4 . The critical wavenumber k_c is also displayed.

where k is the wavenumber, ω is the angular frequency, $X = \epsilon(x - c_g t)$, $\tau = \epsilon^2 t$, A is the amplitude of the wave envelope and c_g is the group speed. Here we omit the derivation and only show the major results. The reader may refer to (22, 23) for more details.

At the linear order $O(\epsilon)$, as expected, one recovers the linear dispersion relation (2.12). At the quadratic order $O(\epsilon^2)$, the explicit form of the group speed c_g is obtained

$$c_g = \frac{d\omega}{dk} = \frac{1 + 3k^2 - 2E_b k}{2\omega}. \quad (2.15)$$

It is equal to the phase speed c_p at the wavenumber $k = k_c$ where c_p attains its minimum denoted by c_{\min} . As already mentioned, such a critical point is a candidate bifurcation point of solitary wavepackets. The type of solitary waves found can be predicted by the type of the associated Nonlinear Schrödinger Equation, given by

$$iA_\tau + \beta A_{XX} + \mu |A|^2 A = 0, \quad (2.16)$$

The coefficients are recovered at cubic order $O(\epsilon^3)$, and were found by (22, 23) to be

$$\beta = \frac{1}{2\sqrt{2 - E_b}} \quad \text{and} \quad \mu = \frac{[4(E_b - 1)^2 - \frac{5}{4}]}{\sqrt{2 - E_b}}, \quad \text{at } k = k_c, \quad (2.17)$$

From (2.17), it can be deduced that

1. when $0 \leq E_b < 1 - \sqrt{5}/4$ or $1 + \sqrt{5}/4 < E_b < 2$, the NLS is of focussing type and predicts the existence of bright solitons.
2. when $1 - \sqrt{5}/4 < E_b < 1 + \sqrt{5}/4$, the NLS is of defocussing type and predicts the existence of dark solitons.

In the former case, which includes the classical capillary-gravity waves ($E_b = 0$), the NLS

equation has explicit bright solitary wave solutions given by

$$A(X, \tau) = \sqrt{\frac{2\alpha}{\mu}} \operatorname{sech} \left(\sqrt{\frac{\alpha}{\lambda}} X \right) e^{i\alpha\tau}, \quad (2.18)$$

$$\zeta = 2\epsilon \sqrt{\frac{2\alpha}{\mu}} \operatorname{sech} \left(\sqrt{\frac{\alpha}{\lambda}} \epsilon(x - c_g t) \right) \cos \left(k(x - c_p t) + \alpha\epsilon^2 t \right) + O(\epsilon^2), \quad (2.19)$$

with a speed-amplitude relation given by

$$a = \sqrt{\frac{8k_c \Delta c}{\mu}} + O(\Delta c), \quad (2.20)$$

where $\Delta c = c - c_{\min}$ and a is the wave amplitude defined by $(\max \zeta - \min \zeta)/2$. It is found that fully nonlinear solitary wavepackets bifurcating from infinitesimal periodic waves at $c = c_{\min}$ are well approximated at small amplitudes (up to $O(\epsilon^2)$) by the NLS solution. For the defocussing case, which for this problem requires the inclusion of the electric field, **(23)** studied the local bifurcation by a reduced model which approximates (2.1)-(2.7). They found that solitary wave solutions about the bifurcation point c_{\min} are dark solitary waves, whose speeds c satisfy $c > c_{\min}$. As the amplitude increases, the solution branches turn in the amplitude-speed parameter space, and eventually the solution branch exits the linear spectrum (i.e. c decreases below c_{\min}). Upon doing so, truly localised solitary wavepackets are found. Their major result can be summarised as in Fig. 3 from **(24)**. As with the focussing case, the bifurcation structure for small amplitudes is predicted by the NLS equation, which has explicit dark solitary wave solutions, given by

$$A(X, \tau) = \alpha \tanh \left(\alpha \sqrt{\frac{\mu}{2\lambda}} X \right) e^{-i\mu\alpha^2\tau}, \quad (2.21)$$

where α is an arbitrary parameter. Combining (2.13) and (2.21) yields the first-order approximation of the solution to the full Euler equations

$$\zeta = 2\epsilon\alpha \tanh \left(\alpha \sqrt{\frac{\mu}{2\lambda}} \epsilon(x - c_g t) \right) \cos \left(k(x - c_p t - \mu\alpha^2\epsilon^2 t) + \varphi \right) + O(\epsilon^2), \quad (2.22)$$

in which φ is the phase. In particular, for dark solitary waves of small amplitude that are symmetric about $x = 0$, it is required that $k = k_c$, $c_p = c_g = c_{\min}$, and $\varphi = \pi/2$ or $3\pi/2$ corresponding to two different families. Dark solitons possess Stokes-like non-decaying oscillations in the far field and travel with speed $c > c_{\min}$. By **(25)**, the speed-amplitude dependence to the leading-order accuracy for Stokes waves or dark solitary waves is given by

$$a = \sqrt{\frac{4k_c \Delta c}{\mu}} + O(\Delta c). \quad (2.23)$$

It is noted that (2.23) is obtained by solving the associated elliptic eigenvalue problem (see **(27)** for more details).

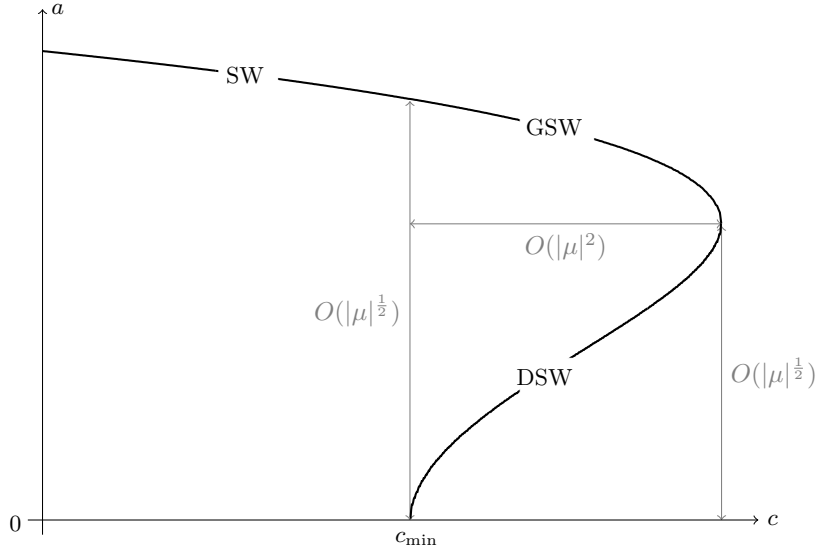


Fig. 3 Schematic of local bifurcation diagram in the case of defocussing NLS. The horizontal scale is exaggerated for a better display. SW, GSW, DSW stand for solitary waves, generalised solitary waves and dark solitary waves respectively.

It is worth mentioning that the existence of solitary wave which bifurcate at finite amplitude does not violate the NLS theory that is only valid for waves of small amplitude. We choose the parameter E_b such that the region of parameter space in which dark solitary waves (DSW) and generalised solitary waves (GSW) is not narrow, and the amplitude of the solitary waves (SW) is not large. This is dependent on the parameter μ from (2.17), as shown in Fig. 3. To this end, we consider the defocussing case with $E_b = 0.6$ in the rest of the paper.

To investigate the global bifurcation, we compute for the fully nonlinear dark solitary waves with the help of the approximated solutions (2.22) as an initial guess in an iterative scheme. The computations are achieved by a boundary integral method that will be presented in the following section.

3. Numerical scheme

To solve for the fully nonlinear system shown in section 2, we follow previous authors (29, 30, 32) and exploit the theory of complex analysis to express unknowns in terms of values on the boundary, and hence reduce the dimension of the problem. We introduce the streamfunction ψ , which is the complex conjugates of ϕ , and hence they satisfy the Cauchy Riemann equations, given by

$$\phi_x = \psi_y, \quad \phi_y = -\psi_x. \quad (3.1)$$

We also introduce a real function w , such that v is the complex conjugate of w . This gives us that

$$w_x = v_y, \quad w_y = -v_x. \quad (3.2)$$

We denote by F and G the complex fluid and electric potentials. That is, $F = \phi + i\psi$, and $G = w + iv$, are both analytic functions of the complex displacement $z = x + iy$. Instead of seeking the potentials in the physical space, we solve for physical variables in the two potential spaces. One does this by taking ϕ and ψ as independent variables, and in the fluid region seek x and y as functions of ϕ and ψ . Meanwhile, in the gas, we seek x and y as functions of the independent variables w and v . The advantage of solving the system in the potential space, rather than the physical space, is that the unknown free boundary is given by equipotentials of both ψ and v .

We seek a steady periodic disturbance of non-dimensional wavelength λ , which is chosen to be large, since we are approximating solitary waves as long periodic waves. When computing dark solitary waves near the bifurcation point predicted by the NLS theory, one must be careful with the choice of λ . The wavelength of the carrier wave in equation (2.22) is 2π , and combined with the phase-shift of π , we must choose $\lambda \approx (2n + 1)\pi$, with n an integer (see, for example, (25)).

Equations (2.3) and (2.5) imply that the fluid and gaseous regions are conformally mapped to Ω_f and Ω_g respectively, where

$$\Omega_f = \{(\phi, \psi); \psi < 0, -c\lambda/2 \leq \phi < c\lambda/2\}, \quad (3.3)$$

$$\Omega_g = \{(w, v); v > 0, -\lambda/2 \leq w < \lambda/2\}. \quad (3.4)$$

We conformally map Ω_f and Ω_g to unit circles in the s and t planes respectively. This is done via

$$s = \exp\left(\frac{kF}{c}\right), \quad t = \exp(kG). \quad (3.5)$$

We introduce two complex analytic functions Γ and Λ , defined by

$$\Gamma = x_\phi - \frac{1}{c} + iy_\phi, \quad (3.6)$$

$$\Lambda = x_w - 1 + iy_w. \quad (3.7)$$

We capitalize functions evaluated on the free boundary, for example $x(\phi, \psi)|_{\psi=0} = X_\phi(\phi)$. We apply Cauchy's integral theorem to the function Γ on the unit disc traversed in an anti-clockwise direction in the s -plane. Taking the real parts, and after application of the chain rule (see e.g. (26)), one finds that

$$X_\phi(\phi_0) = \frac{1}{c} + \frac{1}{2c\lambda} \text{PV} \int_{-c\lambda/2}^{c\lambda/2} \cot\left(\frac{k}{c}(\phi - \phi_0)\right) Y_\phi d\phi, \quad (3.8)$$

where ϕ_0 is any value of $\phi_0 \in [-c\lambda/2, c\lambda/2)$, and 'PV' stands for Cauchy Principal Value. To handle interpolation between the fluid and gaseous regions on the free boundary, we introduce a function $w = h(\phi)$ which must be found as part of the solution. Applying

Cauchy's integral theorem to the function Λ on the unit disc traversed in an anti-clockwise direction in the t -plane gives, after some algebra,

$$\frac{Y_\phi(\phi_0)}{h_\phi(\phi_0)} = 1 - \frac{1}{2\lambda} \text{PV} \int_{-\lambda/2}^{c\lambda/2} \cot\left(\frac{k}{c}(h(\phi) - h(\phi_0))\right) Y_\phi d\phi. \quad (3.9)$$

Equations (3.8) and (3.9) express unknowns on the boundary in terms of an integral equation involving boundary values. We exploit the assumed symmetry about $x = 0$ to reduce the integrals in equations (3.8) and (3.9) to integrals from $\phi = 0$ to $\phi = c\lambda/2$. We discretise ϕ into N equally spaced mesh points ϕ_I , given by

$$\phi_I = \frac{c\lambda}{2} \frac{I-1}{N-1}, \quad I = 1, 2, \dots, N. \quad (3.10)$$

We decompose Y and h_ϕ into Fourier modes:

$$Y = a_0 + \sum_{n=1}^{N-2} a_n \cos\left(\frac{kn}{c}\phi\right), \quad (3.11)$$

$$h_\phi = \frac{1}{c} + \sum_{n=1}^{N-2} b_n \cos\left(\frac{kn}{c}\phi\right). \quad (3.12)$$

Hence, fixing a property of the wave, such as an amplitude parameter $A = Y(0)$, the resulting numerical problem has $2N - 2$ unknowns: a_n , b_n , c , and the Bernoulli constant B . The coefficient a_0 can be taken to be any value, since it only enters the equation via the dynamic boundary condition, and can be absorbed by the Bernoulli constant ($B \rightarrow B + a_0$). We choose a_0 such that the mean depth of the interface displacement is zero. Derivatives of Y can be found by differentiation (3.11). Given Y_ϕ , one can recover X_ϕ by ensuring equation (3.8) is satisfied. The integral is evaluated at midpoints ϕ_I^M using the trapezoidal rule, where

$$\phi_I^M = \frac{\phi_{I+1} + \phi_I}{2}, \quad I = 1, 2, \dots, N-1. \quad (3.13)$$

Values of X_ϕ can be recovered at the meshpoints ϕ_I using four-point interpolation formulae. We rewrite the Bernoulli equation in terms of our unknowns:

$$\frac{1}{2} (X_\phi^2 + Y_\phi^2)^{-1} (1 - E_b^2 h_\phi^2) - \frac{Y_\phi X_\phi - X_\phi Y_\phi}{(X_\phi^2 + Y_\phi^2)^{3/2}} + Y - B = 0. \quad (3.14)$$

We satisfy equation (3.14) at the $N - 1$ midpoints. Furthermore, we satisfy the integral equation (3.9) at the first $N - 2$ midpoints. Finally, we fix the amplitude of the wave, or some other property such as the speed c , to close the system of $2N - 2$ equations with $2N - 2$ unknowns. We solve this numerical system using Newton-Raphson method, stopping iterations once the residuals are of the order 10^{-11} . The Jacobian matrix is approximated numerically. The method typically converges within five or less iterations. It is checked throughout the calculations that (3.9) is also satisfied at the last midpoint with the same accuracy as at the other mesh points. Using the solutions (2.22) as an initial guess, one can

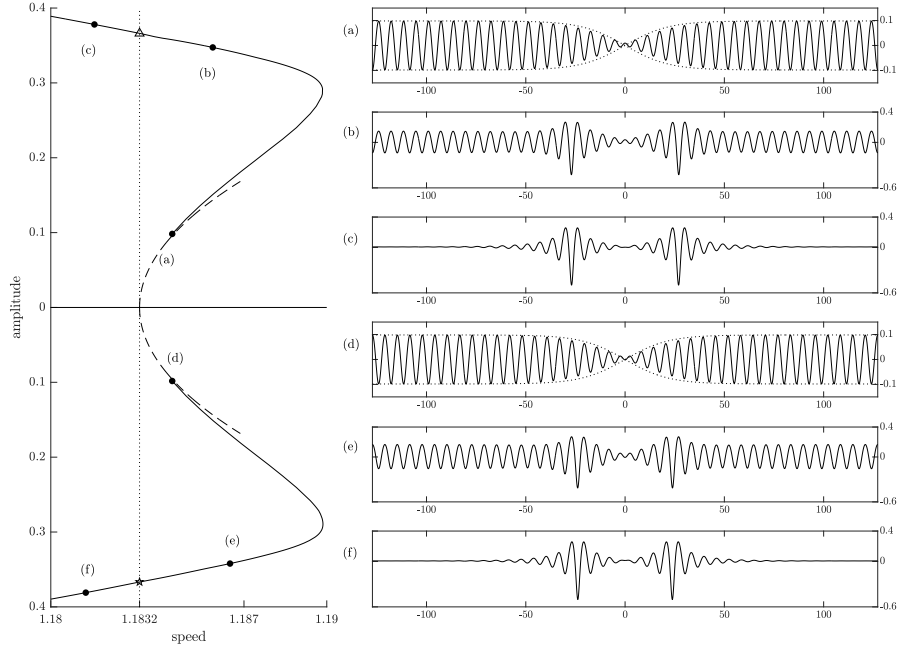


Fig. 4 A local bifurcation diagram for $E_b = 0.6$ and $\lambda = 81\pi$. There is an elevation branch and depression branch, bifurcating from infinitesimal periodic waves. The dashed curves are the NLS prediction, the dotted curve is $c = c_{\min}$, and the triangle and star are used for reference in Fig. 5 and 7. Solutions (a)-(f) are shown in the right-hand panels. The amplitude of the elevation branch is given by $\frac{1}{2}(\max(Y) - \min(Y))$. For the depression branch, we use the negative of this value, to distinguish them clearly on the figure.

find new solutions via the method of continuation. We also note that the complexity of the numerical scheme is of $O(N^3)$.

The above numerical method allows us to explore the fully nonlinear bifurcation diagram of the model presented in section 2. In the following section, we describe the solution space recovered via the fully nonlinear numerical scheme. The accuracy of the numerical procedure is discussed in detail in Appendix A.

4. Fully nonlinear computations

The analysis from section 2 indicated that for small amplitudes, one expects to find two branches of dark solitary waves bifurcating from $c = c_{\min}$. This is indeed the case, and a local bifurcation diagram for $E_b = 0.6$ and $\lambda = 81\pi$ is shown in Fig. 4. Some solutions, denoted (a)-(f) on the branches, are shown in the right-hand panels. The solution branches are completed by a continuation method as presented in the left-hand panels of Fig. 4. The dashed curves are the NLS solution branches, while the solid curves are fully nonlinear

computations. We can see from the NLS solution (2.22) that ζ at $x = 0$ is either a peak (local maximum) or a trough (local minimum). The solutions that have a peak at the point of symmetry are referred to as elevation waves, while those that have a trough are called depression waves. As one moves further along the branch, the profile at $x = 0$ can change from a peak to a trough or vice versa. Nonetheless, we shall refer to the solutions which evolve smoothly from initial elevation waves as the elevation branch as presented in the upper-half of the left panel from Fig. 4. The depression branch is defined similarly and depicted in the lower-half of the left panel from Fig. 4. It can also be seen that for small amplitudes the NLS theory is a very good approximation of the full Euler system. In particular, for solutions (a) and (d) in the figure, the predicted amplitude of the wavepacket is shown by the dashed curves, and is seen to be in very good agreement with the fully nonlinear solutions. However, as the weakly nonlinear assumption becomes further invalidated, the solution branch begins to deviate from the NLS theory. It is found that, like with the model derived in (23), the solution branches turn such that the value of c begins to decrease again towards $c = c_{\min}$. During this process, two depression solitary wave packets form on either side of the point of symmetry $x = 0$ (see solutions (b) and (e)). These are generalised solitary waves: since their speeds are within the linear spectrum of the system, there exists a resonant oscillatory tail. As the solutions cross $c = c_{\min}$, they leave the linear spectrum, and the solutions become localised structures known as bright solitary wavepackets. Solutions (c) and (f) show that they take the form of two depression solitary wavepackets joined together. They are referred to in the literature as multi-packet bright solitary waves. The local bifurcation structure described above is the same as that obtained for the truncated Hamiltonian model in (23).

Next, we explore the global bifurcation structure. In other words, we want to find out what happens to the solitary waves as one continues further along the branches. First, we consider the elevation branch, which is shown in Fig. 5. The branch is shown in a three-dimensional parameter space, starting from the triangle shown in Fig. 4. The parameter \hat{y} is the value of ζ at $x = 0$. The speed is the value c , and the plane $c = c_{\min}$ is given by the grey shaded region. The parameter S is an artificial parameter not related to any physical parameter of the solutions: it is the total arclength of the solution branch itself. We introduce it for aesthetic reasons, allowing us to ‘unfold’ a solution branch which otherwise crosses itself many times. As shown previously, solution (c) in Fig. 4 is a bright multi-packet solitary wave, formed of two depression solitary waves joined together. As one follows the branch, the speed decreases until a point where it turns such that the speed begins to increase again. During this process, the solution at the point of symmetry changes from a peak to a trough, and one oscillation is lost between the two solitary packets. For example, Fig. 6 shows a half wavelength of solutions (c) and (i), given by the solid and dashed curves respectively. It can be seen in the left-hand panel that the depression packet is closer to $x = 0$ for the solution (i). The right-hand panel shows a blow up of the solution near $x = 0$, showing the change at $x = 0$ as it goes from a peak to a trough. Following the branch further, it again crosses $c = c_{\min}$, such that the solutions become generalised solitary waves. The branch again turns, and in the process the two depression packets become elevation packets, as seen in the solution denoted (iii). The branch proceeds to exit and enter the linear spectrum two more times. Each time the branch turns with $c < c_{\min}$, the nature of the solution at $x = 0$ changes from a peak to a trough (or vice versa), and an oscillation is lost between the two packets. For example, this occurs between solutions

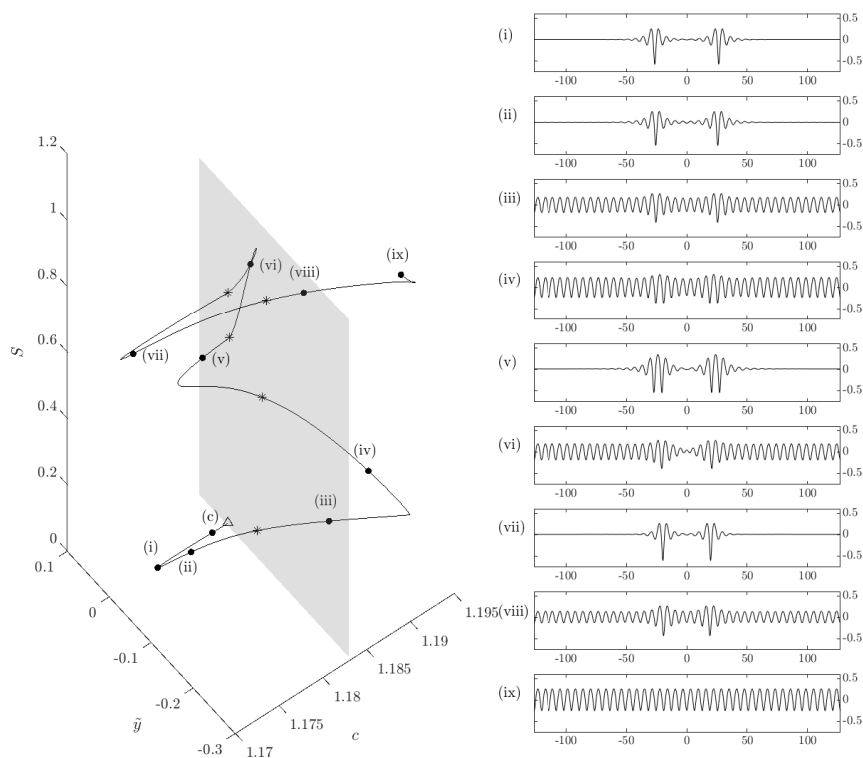


Fig. 5 Global bifurcation diagram of the elevation branch with $E_b = 0.6$ and $\lambda = 81\pi$. The triangle corresponds to the triangle seen in Fig. 4. The grey plane is given by $c = c_{\min}$. Asterisks correspond to points where the solution branch crosses $c = c_{\min}$. The parameter \hat{y} is ζ at $x = 0$, and the parameter S is the arclength of the solution branch itself.

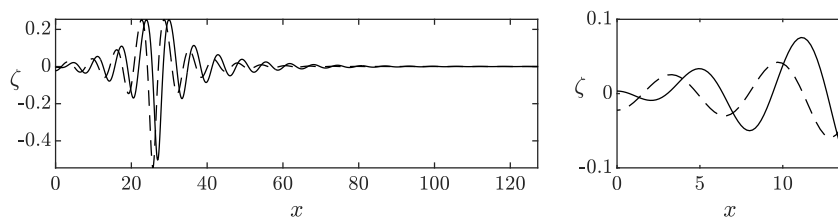


Fig. 6 Solutions (c) and (i) are given by the solid and dashed curves respectively. The left-hand panel shows the solutions over a half wavelength. The right-hand panel is a blow up of the solution at $x = 0$.

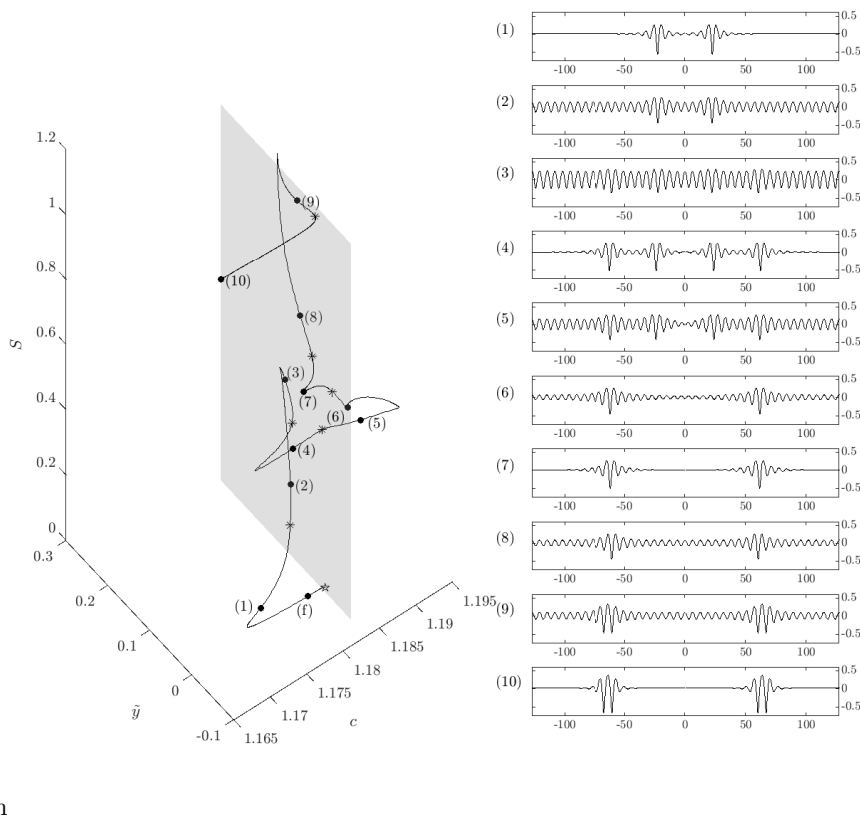


Fig. 7 Global bifurcation diagram of the depression branch with $E_b = 0.6$ and $\lambda = 81\pi$. The star corresponds to the star seen in Fig. 4. The grey plane is given by $c = c_{\min}$. Asterisks correspond to points where the solution branch crosses $c = c_{\min}$. The parameter \hat{y} is ζ at $x = 0$, and the parameter S is the arclength of the solution branch itself.

(iv) and (v). When the branch turns in the region $c > c_{\min}$, the nature of the packets changes. For example, between solution (ii) and (iii), the packets go from depression to elevation. Between solutions (v) and (vi), they revert back from elevation to depression. The final time they re-enter the linear spectrum, the two solitary waves structures are close together (solution (viii)). The solution branch does not turn again, but joins the branch of Stokes wave. Hence, the bifurcation structure is an exotic path through parameter space, connecting an NLS-like dark solitary wave bifurcation about $c = c_{\min}$ to a bifurcation point along the branch of Stokes's waves with periodic 2π .

Next, we consider the depression branch, shown in Fig. 7. The star in the figure is the one previously shown in the local bifurcation diagram in Fig. 4. As with the elevation branch, after crossing $c = c_{\min}$ for the first time, the solution has become a multi-packet

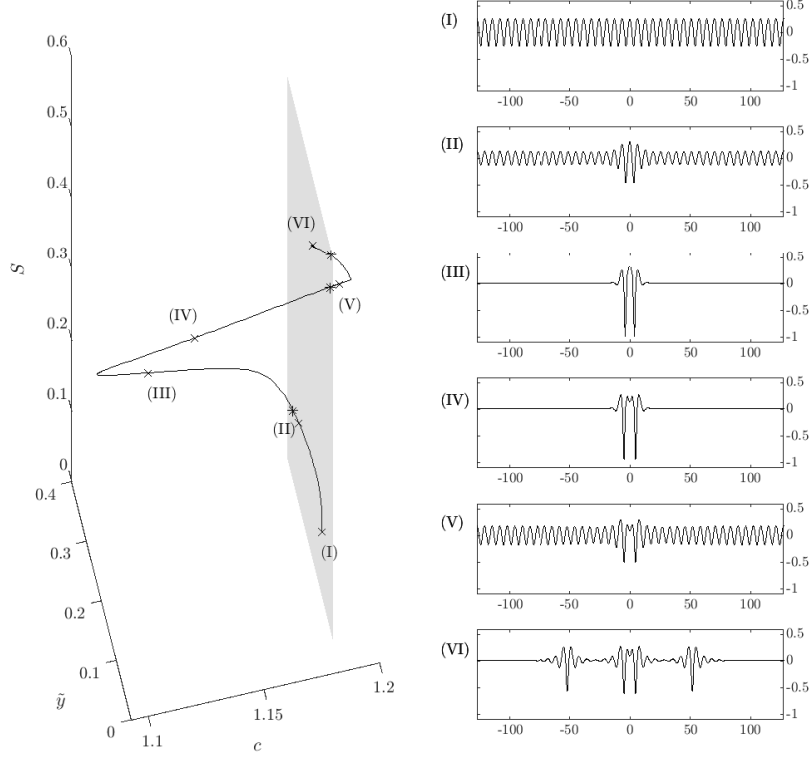


Fig. 8 A solution branch containing single elevation packets, with $E_b = 0.6$ and $\lambda = 81\pi$. The branch is presented in three-dimensional parameter space, where \hat{y} and S are as given in Fig. 5 and 7. The grey plane is $c = c_{\min}$, and the stars correspond to the points where the branch crosses the grey plane. Solutions (I)-(VI) are shown in the right-hand panels.

bright solitary wave, where both packets are of depression, such as solution (*f*). The branch again turns, and passes back through $c = c_{\min}$, where, like the elevation branch from Fig. 5, an oscillation has been lost between the two packets as the branch turns. The solution branch then proceeds to re-enter and exit the linear spectrum three more times. Unlike the elevation branch, upon re-entering and exiting for the first time, the solution does not change from two depression packets to two elevation packets, but rather becomes four depression packets! This can be seen in the evolution of the solution branch between solutions (2) to (4) in Fig. 7. The second time it enters and exits, the two depression packets nearest to each other are lost, seen in solutions (5) and (6). The final time it enters and exits, the two depression packets become elevation packets (see solutions (7) to (10)). The two elevation waves observed in solution (10) are far apart. Computing solutions beyond this

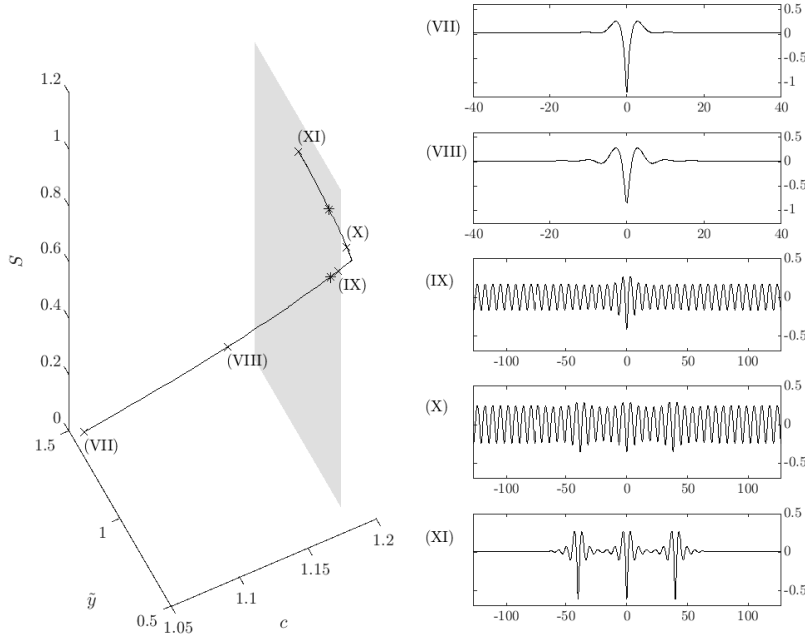


Fig. 9 A solution branch containing single depression packets, with $E_b = 0.6$ and $\lambda = 81\pi$. Solutions (VII)-(XI) are shown in the right-hand panels. Solutions (VII)-(VIII) are shown with a shorter x scale than (IX)-(XI), to make the features of the wave more visible. The grey plane is $c = c_{\min}$, and the stars correspond to the points where the branch crosses the grey plane.

point becomes impractical, due to the large computational domain required, and instead we explore the solution branch for a single elevation packet in the paragraph below. We recomputed the above branch with $\lambda = 101\pi$, to ensure that domain size did not affect the number of solitary packets that formed, such as the four packets in solution (4). The results were in agreement.

The solutions as seen thus far have followed from the global bifurcation of dark solitary waves. We saw that solutions became multi-packet solitary waves. It was shown by (23) that single wave packets could also be found in a defocussing regime, but that they bifurcated at finite amplitude. Further evidence to support this is solution (10) from Fig. 7, where the two elevation packets are very far apart. In Fig. 8 and 9, we present a branch of solutions containing a single elevation and a single depression wavepacket solution respectively. We begin by discussing the branch containing an elevation wavepacket, such as solution (III). Like in (23), it is found that a single elevation solitary wave packet emerges from a branch of generalised solitary waves, e.g. solution (II), which in turn bifurcated from a Stokes wave, shown by solution (I). If we instead follow the solution branch the other way, more single packet elevation solutions, such as (IV), are discovered. The branch enters $c > c_{\min}$,

where one finds that the solution becomes a multi-packet generalised solitary wave, as shown by solution (V). This solution then again leaves the linear spectrum, resulting in a multi-packet solitary wave (VI). We cease our computations here: it has already been seen that multi-packet solutions form long winding paths in parameter space, with the emergence and disappearance of additional packets. Next, consider the branch from Fig. 9. Starting from a depression wavepacket, given by solution (VIII), the amplitude increases one way along the branch. Solution (VII) is as far along the branch as we were able to compute. Past this point, the numerical method becomes stiff, and the iterative procedure fails to achieve satisfactory convergence. The limiting configuration of such a branch remains an open problem. For the case of gravity-capillary surface waves, it is known depression solitary wavepackets in infinite depth water overturn and form a trapped bubble (36). However, due to the presence of the electric field in this model, one cannot smoothly follow the solution branch to the point of a trapped bubble. Going the other way along the branch, the solution enters the linear spectrum resulting in generalised solitary waves as shown in (IX) due to the resonance with periodic waves. Then the solution forms a multi-packet structure, given by solution (X). We compute the branch as far as solution (XI), where the branch again exits the linear spectrum, and becomes three depression packets.

5. Conclusion

In conclusion, we have presented the global bifurcation structure of EHD solitary waves travelling on the interface between a conducting fluid and a dielectric gas. The results are an extension of the work of (23), where the new fully nonlinear computations presented here allow us to explore the solitary wave branches into strongly nonlinear regimes. The inclusion of the electric field allows for the associated NLS equation to be of the defocussing type at the minimum of the dispersion relation. This occurs for the parameter range $1 - \sqrt{5}/4 < E_b < 1 + \sqrt{5}/4$, motivating the choice $E_b = 0.6$ as the parameter for which we presented solution branches. Two branches of dark solitary waves bifurcate at zero amplitude about the minimum of the dispersion relation (2.12). The branches were then found to enter and exit the linear spectrum of the system a number of times. The solutions observed along the branch are rather exotic, where multi-packet solitary waves are formed via the appearance and disappearance of additional wavepackets as the solution branches turn in the linear spectrum. The results presented here are the first to show the global bifurcation structure of a fully nonlinear water wave system which is approximated by a defocussing NLS for small amplitude. Previously, this was attempted for flexural-gravity waves by (25), but higher order derivatives in the boundary condition made the numerical method too stiff to follow the branches very far. We also found that the single packet solutions found in a defocussing regime exist on branches that pass through $c = c_{\min}$, and along which more multi-packet solutions are found.

A very recent work (37) by Wang proposed a novel Whitham-type model equation that can capture the essential features of a bifurcation mechanism in the defocussing NLS framework for the problem of hydroelastic waves. Such model is also valid for investigating the present problem in electrostatics. This will be left for future work.

Acknowledgement

The work was achieved during a collaborative research visit of A.D. at University of Greenwich sponsored by the *QJMAM* fund for Applied Mathematics (A.D.). T. G. was

sponsored by the Numerical and Applied Mathematics Research Unit (NAMU), University of Greenwich. We thank the referees for their insightful comments, and helping to improve the quality of the paper.

References

1. S. F. Kistler & P. M. Schweizer, *Liquid film coating - scientific principles and their technological implications*, Chapman and Hall, 1997.
2. E. M. Griffing, S. G. Bankoff, M. J. Miksis & R. A. Schluter, Electrohydrodynamics of thin flowing films, *J. Fluids Eng.* **128** (2006) 276–283.
3. G. I. Taylor & M. D. Van Dyke, Electrically Driven Jets. *Proc. Roy. Soc. A*, **313** (1969) 453–475.
4. U. Ghoshal & A. C. Miner, Cooling of high power density devices by electrically conducting fluids. *U.S. Patent* (2003) 6,658,861.
5. X. Chen, & J. Cheng, and X. Yin. Advances and applications of electrohydrodynamics. *Chin. Sci. Bull.* **48** (2003): 1055–1063.
6. D. T. Papageorgiou, Film Flows in the Presence of Electric Fields. *Ann. Rev. Fluid Mech.* **51** (2019) 155–187.
7. G. Taylor & A. McEwan, The stability of a horizontal fluid interface in a vertical electric field, *J. Fluid Mech.* **22** (1965) 1–15.
8. J. R. Melcher & W. J. Schwarz, Interfacial relaxation overstability in a tangential electric field, *Phys. Fluids* **11** (1968) 2604–2616.
9. N. M. Zubarev & E. Kochurin, Nonlinear dynamics of the interface between fluids at the suppression of Kelvin-Helmholtz instability by a tangential electric field, *JETP letters* **104** (2016) 275–280.
10. L. L. Barannyk & D. T. Papageorgiou & P. G. Petropoulos, Suppression of Rayleigh-Taylor instability using electric fields, *Math. Comp. Simul.* **82** (2012) 1008–1016.
11. R. Cimpeanu, D. T. Papageorgiou, P. G. Petropoulos, On the control and suppression of the Rayleigh-Taylor instability using electric fields, *Phys. Fluids* **26** (2014) 022105.
12. J. Hunter & J.-M. Vanden-Broeck, Solitary and periodic gravity-capillary waves of finite amplitude. *J. Fluid Mech.*, 134 (1983), 205–219.
13. J.-M. Vanden-Broeck, Elevation solitary waves with surface tension. *Phys. Fluids*, **3** (1991), 2659–2663.
14. F. Dias, Capillary-gravity periodic and solitary waves. *Phys. Fluids*, 6(7) (1994) 2239–2241.
15. F. Dias, F., D. Menasce & J.-M. Vanden-Broeck, Numerical study of capillary-gravity solitary waves. *Eur. J. Mech. B-Fluid.*, **15**(1) (1996), 17–36.
16. D. Clamond, D. Dutykh & A. Durán, A plethora of generalised solitary gravity-capillary water waves. *J. Fluid Mech.* **784** (2015), 664–680.
17. Z. Wang, J.-M. Vanden-Broeck & P. A. Milewski, Asymmetric gravity-capillary solitary waves on deep water. *J. Fluid Mech.*, **759** (2014).
18. T. Gao, Z. Wang & J.-M. Vanden-Broeck, On asymmetric generalized solitary gravity-capillary waves in finite depth, *Proc. R. Soc. A* **472** (2016) 20160454.
19. Z. Wang, Stability and dynamics of two-dimensional fully nonlinear gravity-capillary solitary waves in deep water. *J. Fluid Mech.*, **809**, (2016) 530–552.
20. H. Gleeson, P. Hammerton, D. Papageorgiou, J.-M. Vanden-Broeck, A new application

- of the Korteweg-de Vries Benjamin-Ono equation in interfacial electrohydrodynamics, *Phys. Fluids* **19** (2007) 031703.
21. M. Hunt, J.-M. Vanden-Broeck, D. T. Papageorgiou, E. Părău, Benjamin-Ono Kadomtsev-Petviashvili's models in interfacial electro-hydrodynamics, *Eur. J. Mech.-B/Fluids* **65** (2017) 459–463.
 22. Z. Wang, Modelling nonlinear electrohydrodynamic surface waves over three-dimensional conducting fluids, *Proc. Roy. Soc. A* **473** (2200) (2017) 20160817.
 23. Z. Lin, Y. Zhu, & Z. Wang, Local bifurcation of electrohydrodynamic waves on a conducting fluid. *Phys. Fluids*, **29**(3) (2017) 032107.
 24. T. Gao, P. A. Milewski, & J.-M. Vanden-Broeck, Hydroelastic solitary waves with constant vorticity. *Wave Motion*, **85** (2019) 84–97.
 25. P. A. Milewski, J.-M. Vanden-Broeck & Z. Wang, Steady dark solitary flexural gravity waves. *Proc. R. Soc. A* **469** (2013) 20120485.
 26. F. G. Tricomi, *Integral equations*, Vol. **5** (1985), Courier corporation.
 27. Z. Wang & P. A. Milewski, Dynamics of gravity-capillary solitary waves in deep water. *J. Fluid Mech.*, **708** (2012) 480–501.
 28. D. T. Papageorgiou, P. G. Petropoulos & J.-M. Vanden-Broeck, Gravity capillary waves in fluid layers under normal electric fields. *Phys. Rev. E*, **72** (2005) 051601.
 29. D. T. Papageorgiou, & J.-M. Vanden-Broeck, Numerical and analytical studies of nonlinear gravity-capillary waves in fluid layers under normal electric fields. *IMA J. Appl. Math.*, **72** (2006) 832–853.
 30. T. Gao, P. A. Milewski, D. T. Papageorgiou, & J.-M. Vanden-Broeck. Dynamics of fully nonlinear capillary-gravity solitary waves under normal electric fields. *J. Eng. Math.* **108** (2018) 107–122.
 31. T. Gao, A. Doak, J.-M. Vanden-Broeck & Z. Wang, Capillary-gravity waves on a dielectric fluid of finite depth under normal electric field, *Eur. J. Mech. B* **77** (2019) 98–107.
 32. A. Doak, T. Gao, , J.-M. Vanden-Broeck & J. J. S. Kandola, Capillary-gravity waves on the interface of two dielectric fluid layers under normal electric fields. *Q. J. Mech. Appl. Math.* **73** (3) (2020) 231-250.
 33. T. R. Akylas, Envelope solitons with stationary crests, *Phys. Fluids A* **5** (4) (1993) 789-791.
 34. G. Xu & Z Lin, Bifurcation mechanism of interfacial electrohydrodynamic gravity-capillary waves near the minimum phase speed under a horizontal electric field. *Theor. App. Mech. Letters* **11** (2) (2021) 100224
 35. J.-M. Vanden-Broeck, Elevation solitary waves with surface tension. *Phys. Fluids A* **3** (11) (1991) 2659-2663.
 36. J.-M. Vanden-Broeck & F. Dias, Gravity-capillary solitary waves in water of infinite depth and related free-surface flows. *J. Fluid Mech.*, **240** (1992) 549–557.
 37. Z. Wang, A universal bifurcation mechanism arising from progressive hydroelastic waves. *Theo. Appl. Mech. Lett.*, (2021), 100315.
 38. Z. Wang & J.-M. Vanden-Broeck, . Multilump symmetric and nonsymmetric gravity-capillary solitary waves in deep water. *SIAM J. Appl. Math.*, **75**(3) (2015) 978–998.

N	(a)	(b)	(c)	speed of one iteration (in seconds)
200	-0.00826	-0.00320	0.00188	~ 0.1
400	-0.00934	-0.00456	0.00176	~ 1
800	-0.00944	-0.00469	0.00175	~ 8
1600	-0.00945	-0.00470	0.00175	~ 60

Table A Values of a_1 obtained for different N for solutions (a) – (c) shown in Fig. 4. A typical time for one iteration is also presented.

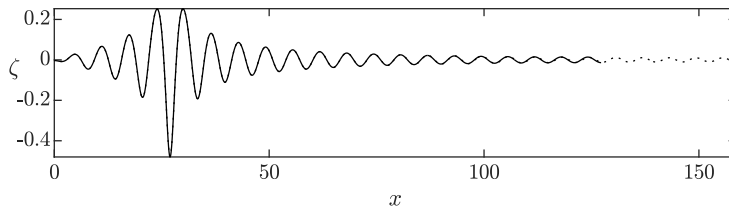


Fig. A Solution with $c = c_{\min} - 10^{-5}$ for $\lambda = 81\pi$ (solid curve) and $\lambda = 101\pi$ (dotted curve). Only half a wavelength is shown. Since neither solution has yet decayed to a flat far-field, they are periodic solutions, rather than bright solitary waves.

In this appendix, we discuss the accuracy and the efficiency of the numerical procedures. Consider first the consequence of varying the number of mesh points used. We computed solutions (a) – (c) from Fig. 4 for different values of N . We fix the speed c , and present the first Fourier mode a_1 from equation (3.11) in Table A. The table demonstrates the convergence of the numerical method as N increases. The computational times confirm the $O(N^3)$ -complexity. One can also check the order of magnitude of the coefficients a_n . For solution (c), we find that $a_{100} \sim 10^{-4}$, $a_{200} \sim 10^{-7}$, $a_{400} \sim 10^{-10}$, and $a_{600} \sim 10^{-13}$. Most solutions presented in this paper are computed with $N = 800$, which we found to be a good compromise between accuracy and speed of computation.

In this paper, we explored solitary waves and generalised solitary waves. However, it was found that for solutions close to $c = c_{\min}$, the decay of the solitary wave packet is very slow. This is predicted at small amplitude by the NLS theory. When the NLS is focussing, bright solitary waves are given by (2.18), with speed given by (2.20). As $c \rightarrow c_{\min}$, the coefficient $\alpha \rightarrow 0$, resulting in a slow decay in the wavepacket solution (2.18). Likewise, the same behaviour is observed for the dark solitary waves of the defocussing NLS, as seen in equations (2.22) and (2.23). This slowly decaying behaviour near $c = c_{\min}$ persists into strongly nonlinear regimes. For example, in Fig. A, we present a solution from the elevation branch in Fig. 4 with a speed $c = c_{\min} - 10^{-5}$ for two different values of λ . It can be seen that for both $\lambda = 81\pi$ and $\lambda = 101\pi$, the oscillations in the tail have yet to fully decay. Despite this, the solutions are in good agreement up to where the $\lambda = 81\pi$ solution ends. As one computes solutions with yet larger values of L , the amplitude of the oscillations will eventually decay to zero. However, this presents computational impracticality, requiring very large λ for solutions near c_{\min} . Instead, we choose to fix λ (typically $\lambda = 81\pi$, unless stated otherwise), and solutions with $c < c_{\min}$ computed in a region near $c = c_{\min}$ in this paper are not solitary waves, but rather a long periodic wave, which tends to a solitary wave as $\lambda \rightarrow \infty$.

As we have already seen, solutions with $c > c_{\min}$ have oscillatory tails. As explained in section 2, to obtain dark solitary waves near the zero amplitude bifurcation point in Fig. 4, one requires $\lambda \approx (2n + 1)\pi$. As one moves further along the branch, the solutions are no longer well predicted

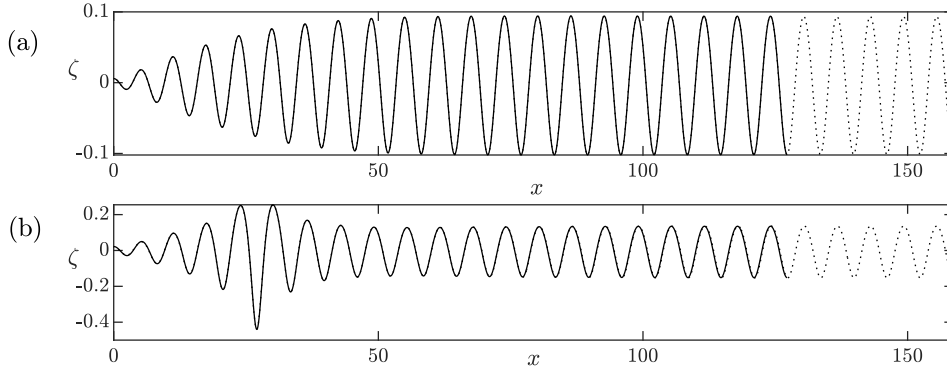


Fig. B Solution (a) and (b) from Fig. 4 for $\lambda = 81\pi$ (solid curve) and $\lambda = 101\pi$ (dotted curve). Only half a wavelength in shown.

the NLS solution (2.22), and the solutions become multi-packet generalised solitary waves, like solutions (b) and (e). Unlike localised structures, generalised solitary waves are known to have dependence on the wavelength of the solution (e.g. (35)). Varying the wavelength affects the wavelength of the oscillatory tail. Since we wish for our solution branches to extend from the dark solitary waves, we choose to fix $\lambda = 81\pi$ for computations along the entirety of the branch. For the generalised solitary waves computed in Fig. 4, varying λ by integers of 2π results in almost overlapping profiles, where the solution with larger λ has additional oscillations of a wavelength of approximately 2π in the tail. This is shown in Fig. B for solutions (a) and (b) from Fig. 4 where the profiles for $\lambda = 81\pi$ and $\lambda = 101\pi$ are shown to be in almost perfect agreement. However, as we explore the global bifurcation structure, multi-packet generalised solitary waves computed further along the branch may not have a resonant tail with a wavelength of approximately 2π . This is because strongly nonlinear wavepackets, unlike weakly nonlinear NLS wavepackets (2.22) and (2.18), do not have decoupled packet amplitude and carrier wave. Nonetheless, one can find, for any generalised solitary wave solution computed in this paper, another generalised solitary wave with a larger wavelength such that the solutions overlap, where the longer solution has additional oscillations in the tail. The dependence of the computational domain for the generalised solitary wave can affect the multi-packet bright solitary wave that emerges as the branch exits the linear spectrum: there can be one extra or one less oscillation between the packets of the solution. All solutions computed retain good convergence as N is increased. In this sense, we believe all of these numerical solutions to be solutions to the original system: multi-packet solutions can be found with different distances between the packets (38).